

Portable Remote Imaging Spectrometer (PRISM): laboratory and field calibration

Pantazis Mouroulis^{*a}, Byron Van Gorp^a, Robert O. Green^a, Michael Eastwood^a, Joseph Boardman^b, Brandon S. Richardson^a, Jose I. Rodriguez^a, Eugenio Urquiza^a, Brian D. Franklin^a, Bo-Cai Gao^c

^aJet Propulsion Laboratory, California Institute of Technology, Pasadena, CA, USA 91109

^bAnalytical Imaging and Geophysics LLC, 4450 Arapahoe Ave. Ste 100, Boulder, CO, USA 80303

^cNaval Research Lab, 4555 Overlook Ave. SW, Washington, DC USA 20375

ABSTRACT

We report the characteristics of the Portable Remote Imaging Spectrometer, an airborne sensor specifically designed for the challenges of coastal ocean research. PRISM has high signal to noise ratio and uniformity, as well as low polarization sensitivity. Acquisition of high quality data has been demonstrated with the first engineering flight.

Keywords: Imaging spectroscopy, coastal ocean, imaging spectrometer

1. INTRODUCTION

The Portable Remote Imaging Spectrometer was conceived in response to a need expressed by the National Aeronautics and Space Administration to provide high quality coastal ocean remote sensing data from an airborne platform with higher temporal and spatial resolution than satellite sensors. PRISM development started in 2009 and was completed in the spring of 2011. The basic design of PRISM has been previously published,¹ as well as modifications to the design that improved manufacturability². This paper will present laboratory measurements demonstrating instrument characteristics as well as limited results from the first engineering flight. A more detailed account will be published in a forthcoming paper.

PRISM comprises an imaging spectrometer covering the near UV to near IR range (350-1050 nm) and a separate spot radiometer covering two short wave infrared (SWIR) bands at 1240 and 1610 nm respectively. An instrument schematic is shown in Fig. 1. Critical aspects of the design are the low F-number (F/1.8) and a total internal reflection prism.

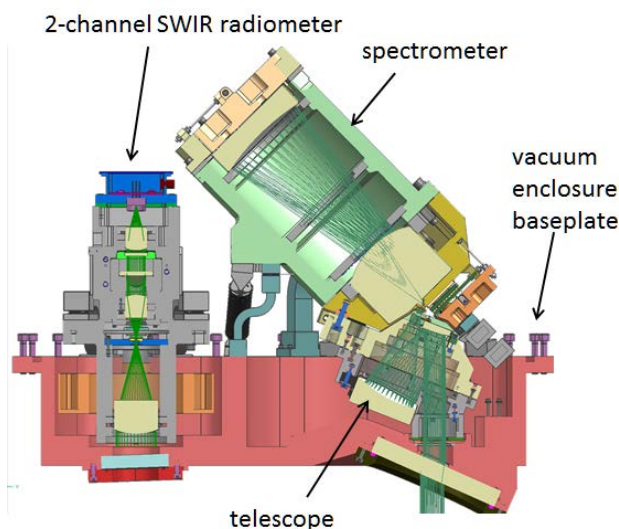


Figure 1. PRISM instrument layout showing the Dyson-type spectrometer, two-mirror telescope, and SWIR radiometer.

[*pantazis.mouroulis@jpl.nasa.gov](mailto:pantazis.mouroulis@jpl.nasa.gov); phone 1 818 393-2599

2. INSTRUMENT DESCRIPTION

The basic instrument parameters and specifications are shown in Tables 1 and 2. These represent measured values, and where slight variations exist, a mean/typical is given.

Table 1. Spectrometer characteristics.

Spectral	Range	350-1050 nm
	Sampling	2.85 nm
	Resolution (FWHM)	3.5 nm
	Calibration uncertainty	<0.1nm
Spatial	Field of view	30.7°
	Instantaneous FOV sampling	0.882 mrad
	IFOV resolution (FWHM)	0.97 mrad
	Cross-track spatial pixels	608
Radiometric	Range	0 to max. beach R
	Sampling	14 bit
	Calibration uncertainty	<2%
	SNR	2000 @450 nm*
	Polarization variation:	<1%
Uniformity	Spectral cross-track uniformity	>95%
	Spectral IFOV mixing uniformity	>95%

*: at a readout rate of 12 fps and 10 nm equivalent bands

Table 2. SWIR Radiometer characteristics.

Parameter	Channel 1	Channel 2
Channel center (nm)	1240*	1610*
Bandwidth (nm)	20*	60*
FOV (mrad, FWHM)	2.4	2.4
Boresight knowledge (mrad, relative to spectrometer)	0.05	0.05
Radiometric stability	99%	99%
SNR @ 1.2mW/cm ² sr	325	390

*: nominal values, for details see next Section.

The complete sensor comprises the optical head assembly (OHA) and control electronics. The OHA comprises the vacuum vessel with the spectrometer and radiometer inside, an aircraft interface/mounting plate, a INS/GPS unit attached to the optical head for enabling precise orthorectification and geolocation, as well as the preamplifier and A-D converter for the detector electronics. The vacuum vessel shell is temperature-stabilized to around 26°C with external strip heaters. Three commercial vibration isolators prevent high frequency vibration from transmitting to the optics and detectors. Figure 2 is a picture of the OHA.

The control electronics are shown in Fig. 3, separated in two racks (though a single rack configuration has also been flown). The control computer passes the high speed data stream to a CORE DVR data recording unit where the data is stored on solid state drives with a total capacity of 1.5Tb. The drives are removed after the flight and the data downloaded to another computer for same-day processing. The remaining electronics are dedicated to thermal control and data logging. The temperature of the instruments inside the vacuum vessel is kept at 25°C through bi-directional thermoelectric coolers. The spectrometer detector is running at a temperature of about 7°C. There are also two shutters, one for the SWIR radiometer and one for the spectrometer that are controlled to provide a dark frames acquisition at the beginning and end of a flight line.

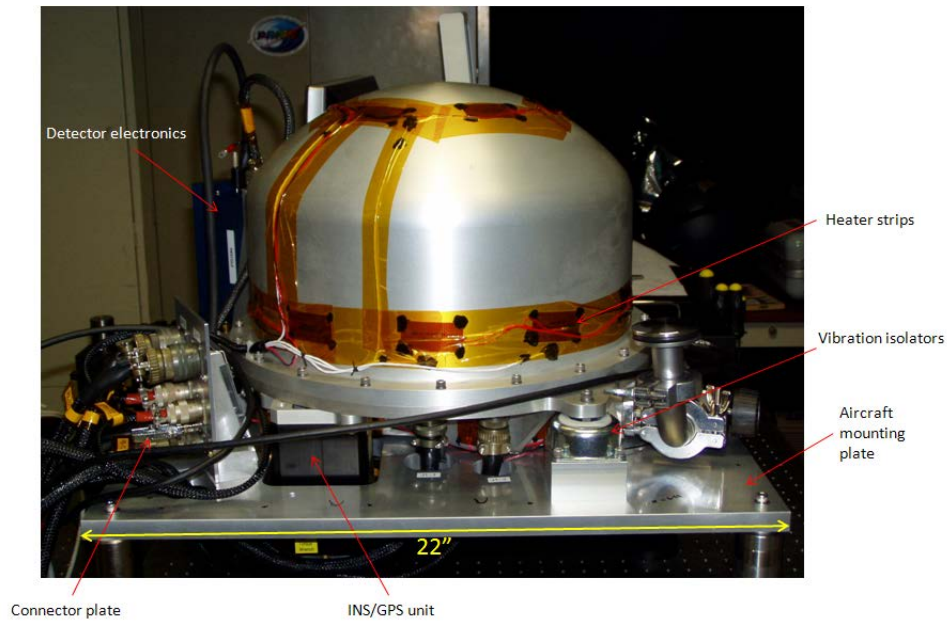


Figure 2. PRISM optical head assembly and aircraft mounting plate.



Figure 3. PRISM control electronics.

3. LABORATORY MEASUREMENTS

PRISM underwent a thorough laboratory evaluation. A representative set of results is given below. Starting with the spectral characteristics, a set of representative spectral response functions is given in Fig. 4, spanning the range 350-450 nm. From this measurement as well as measurements of fixed spectral lines, we established the dispersion to be ~ 2.85 nm/pixel. The actual dispersion value varies slightly with wavelength. The magnitude of this variation is approximately 0.5nm over the entire range. This difference, although small, has an impact in precise calibration and atmospheric correction.

The spectral response functions of Fig. 4 represent raw data normalized to unity at the peak, without Gaussian interpolation or smoothing. Other wavelengths and fields show similar results. The through-field variation of the FWHM remains at or below 10% of a pixel width. Figure 5 is a representation of the spectral alignment and of the curvature of the monochromatic slit image (smile). It can be seen that the smile is very low, and the spectral alignment is 2% of a pixel over the entire field, corresponding to a spectral accuracy of 0.057 nm.

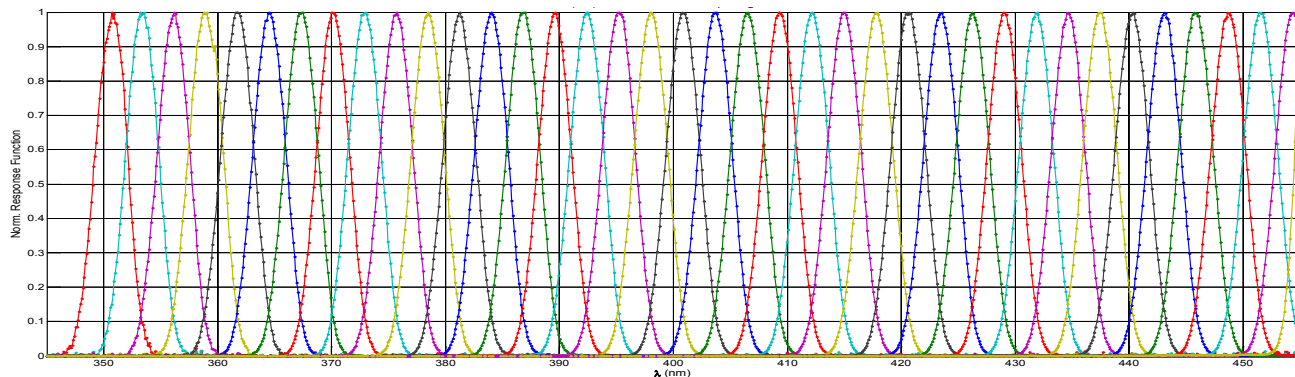


Figure 4. Spectral response functions for the middle of the field of view spanning the range 350 -450 nm.

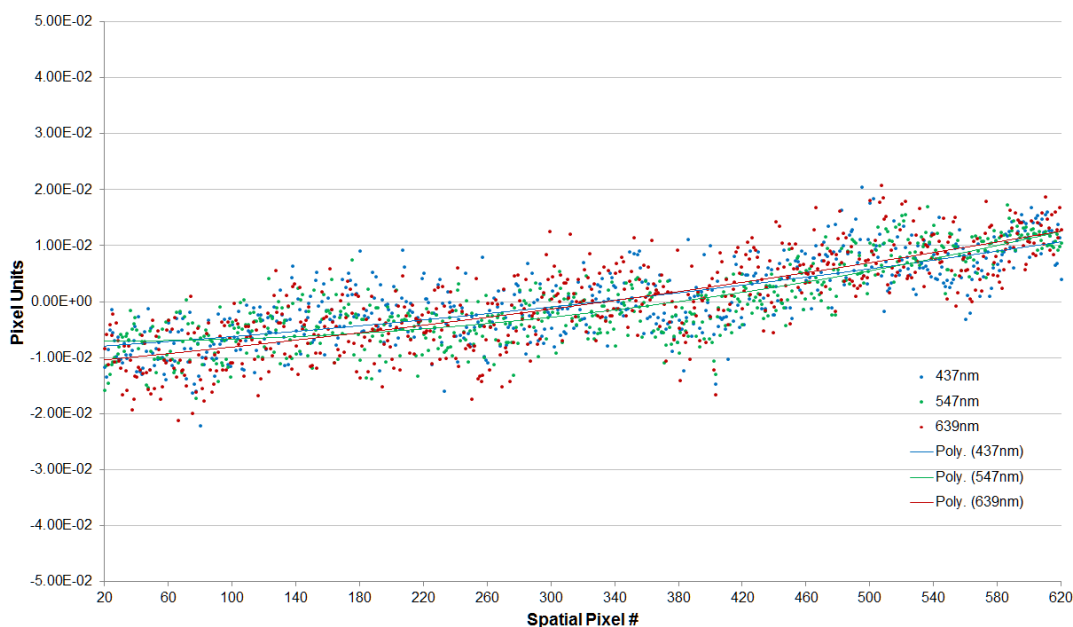


Figure 5. Scatter plot of spectral channel centroids as a function of spatial location for three isolated wavelengths (Hg lamp 437 nm and 547 nm, and laser at 639 nm).

The spatial characteristics of PRISM were established through measurement of the cross-track and along-track spatial response functions (ARF and CRF) through field and wavelength. These are measured by scanning a subpixel slit placed at the focal plane of a collimator illuminating the instrument aperture, and oriented parallel or perpendicular to the spectrometer slit. Representative ARFs are shown in Fig. 6, showing a small to negligible variation both through field and (more importantly) through wavelength. The FWHM of these functions is about 1.1 pixel unit.

Representative CRFs are shown in Fig. 7 for adjacent pixels and wavelengths spanning the spectral range. The FWHM is again around 1.1 pixel units, however a small asymmetric tail is also visible in some functions. The origin of this effect

is electronic rather than optical and can be diminished with further cooling of the detector. However, the effect is rather small and the required cooling significant, so it was not implemented. However, because these functions are not well characterized as Gaussians, we do not characterize the uniformity through the more usual method of keystone and FWHM variation. Instead, we adopt a measure of the total chromatic variation of the CRF integral that extends to the adjacent pixels. This measure, similar to that proposed in ref. 3, contains both center and width variation and makes no assumptions about the shape of the curve. The total maximum integrated variation (nonuniformity) normalized to the CRF integral in the main pixel is <5%.

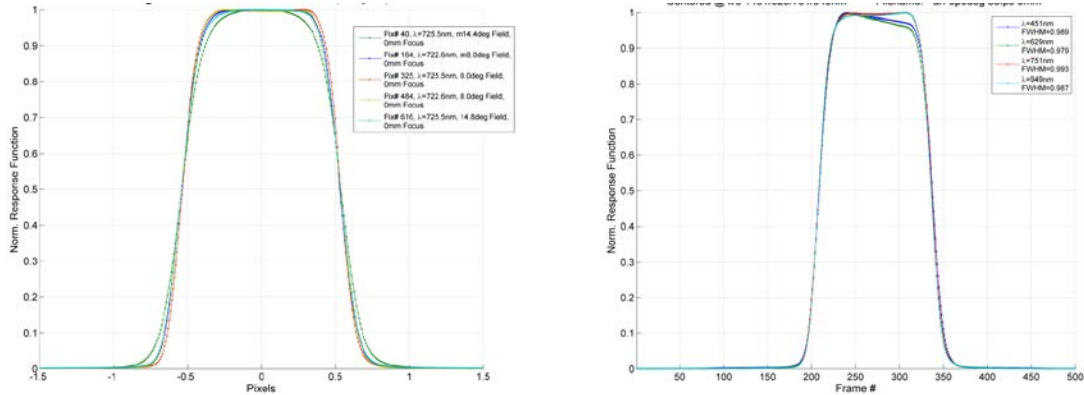


Figure 6. Along-track response functions for several fields and one wavelength (left), and for a single field/several wavelengths (right). The vertical axis is normalized to unity. The horizontal axis has been converted to pixel (slit) width units on the first chart. Motion blur is convolved with these functions in flight.

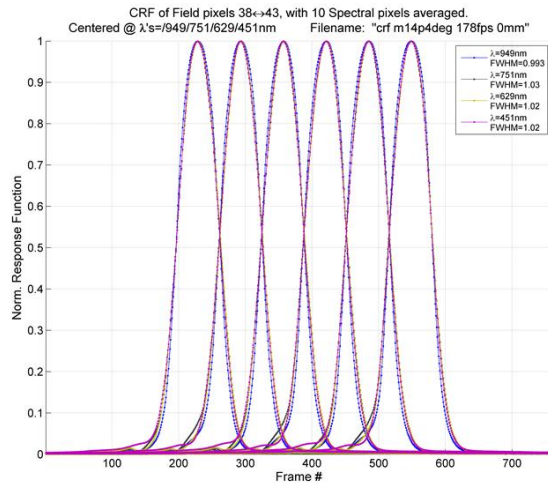


Figure 7. Typical cross-track spatial response functions for adjacent pixels and several wavelengths. The vertical axis is normalized to unity.

PRISM geometric calibration is shown in Fig. 8. The slit image projected on the ground is an arc with a curvature (sag) corresponding to about 0.8° . Measurement and theoretical analysis from the telescope design data agree closely.

The optical design of PRISM was driven by a requirement for low polarization sensitivity, as has been explained in some detail previously². To measure this effect, a tungsten source was used to illuminate an integrating sphere which was placed at a distance of about 1m from the spectrometer. A linear polarizer was placed in front of the spectrometer aperture and rotated. The resulting variation recorded as $(I_{\max} - I_{\min}) / (I_{\max} + I_{\min})$ is plotted as a function of wavelength for five field points in Fig. 9. It can be seen that the variation remains everywhere at or below 1% with the exception of a

spike at around 615 nm. This spike is due to the two-segment order-sorting filter seam. The pixels that are affected by it can be considered as effectively masked, although it is still possible to retrieve useful data from them.

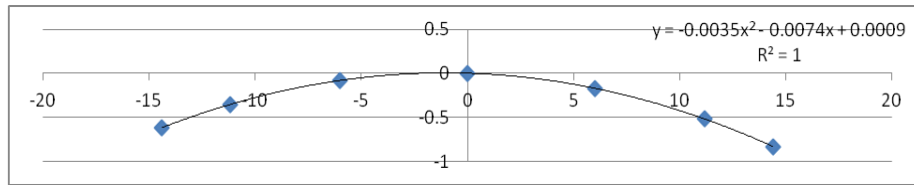


Figure 8. Slit image projected to infinity is slightly curved. The measured data are shown here. For both axes, the units are degrees of angle.

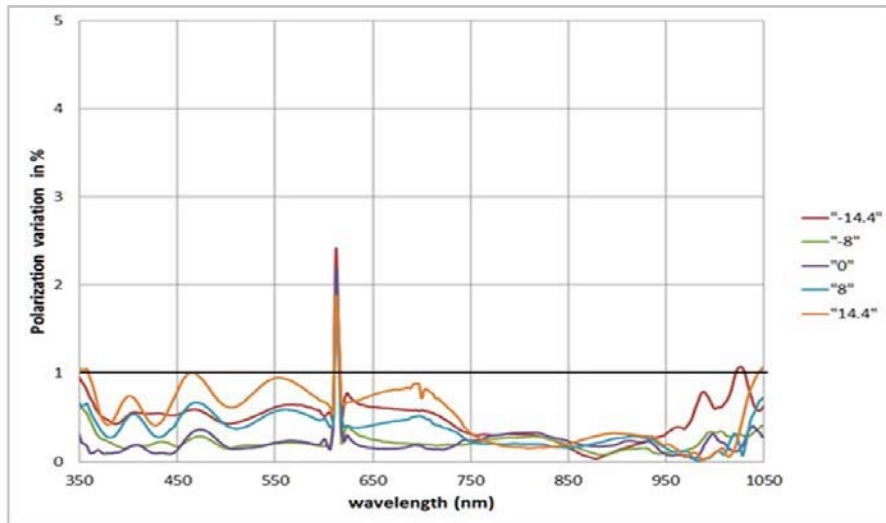


Figure 9. Polarization variation throughout the spectral range for five positions spanning the field of view.

The signal to noise characteristics of the spectrometer were assessed by first measuring signal and noise levels using a source of known radiance (NIST-traceable calibrated lamp, placed at a distance of 0.5m from a calibrated spectralon panel). This was then scaled to signal levels expected in flight. We then summed frames to an equivalent 12 fps rate and resampled the spectral data to 10 nm bands for comparison with previous spectrometers and especially AVIRIS⁴. The result is shown in Fig. 10. The SNR peaks at around 2000 in the region 450-550 nm.

The SWIR radiometer is intended to aid with the atmospheric correction algorithm. It has a field of view of approximately 2mrad and looking towards the middle of the spectrometer FOV. The spatial alignment of the radiometer relative to the spectrometer was obtained by using a large aperture collimator and illuminating both instruments simultaneously. Scanning a slit produced simultaneous ARF and CRF data for the two instruments. The result of this measurement is shown in Fig. 11.

The spectral response of the two SWIR channels is shown in Fig. 12. This was measured with a scanning monochromator and a collimating lens in front of the instrument. Signal to noise measurements were also performed for the SWIR radiometer using techniques similar to those of the spectrometer. The results were shown in Table 2.

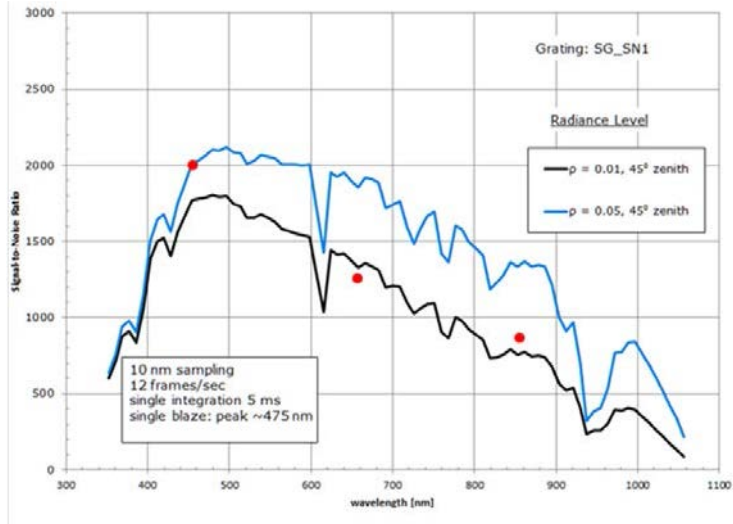


Figure 10. Signal to noise ratio through wavelength for two reference radiances including atmospheric transmittance. Red dots show original PRISM design requirement (relative to top curve) being met or exceeded.

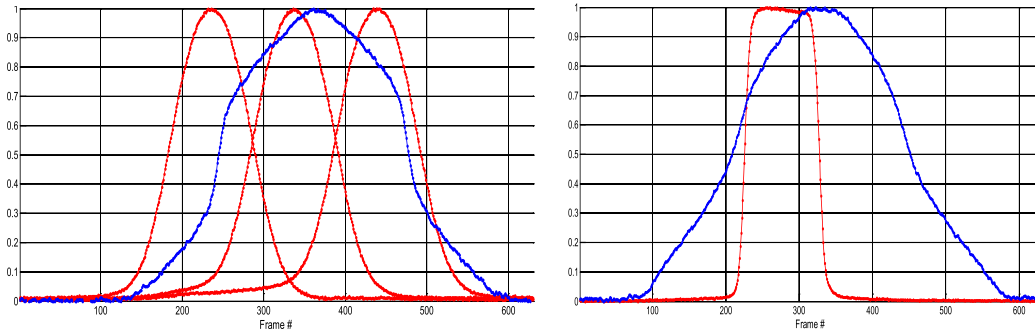


Figure 11. Cross-track (left) and along track (right) spatial response of the SWIR radiometer relative to the spectrometer. On the left, the broader radiometer response is located relative to spatial channels 321-323.

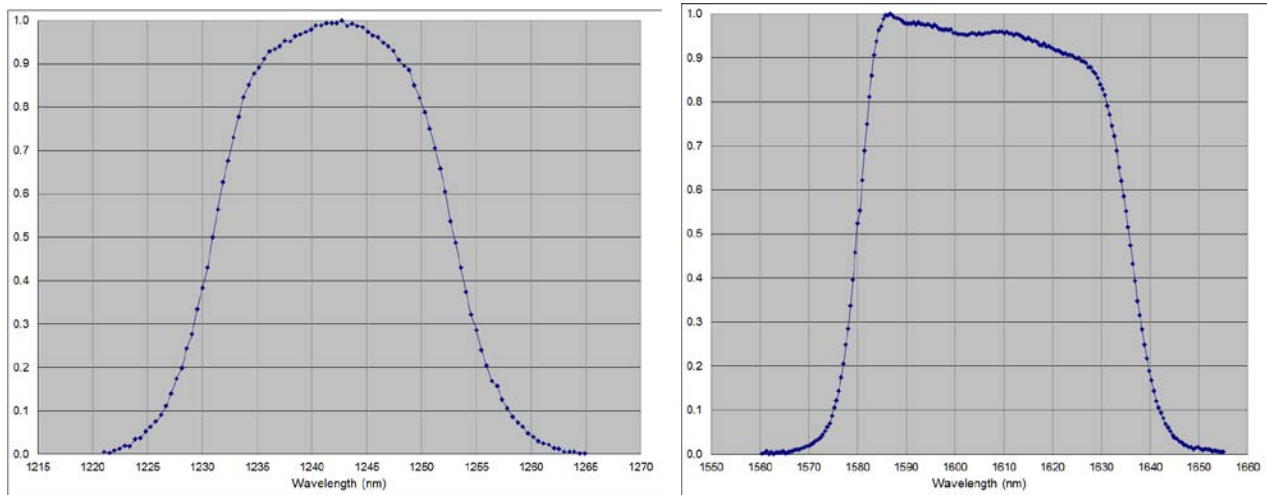


Figure 12. Spectral response of the two SWIR channels, 1240 and 1610 nm.

4. RESULTS FROM FIRST PRISM FLIGHT

PRISM was integrated on the NASA Glen Research Center Twin Otter aircraft for its first engineering flight (Fig. 13). The first test flight was over the JPL campus and local area as the road grid and buildings are an aid to correct image rectification. Figure 14 shows a rectified and geolocated image of the JPL campus and adjacent Arroyo Seco area, demonstrating that the orthorectification algorithm is working properly.

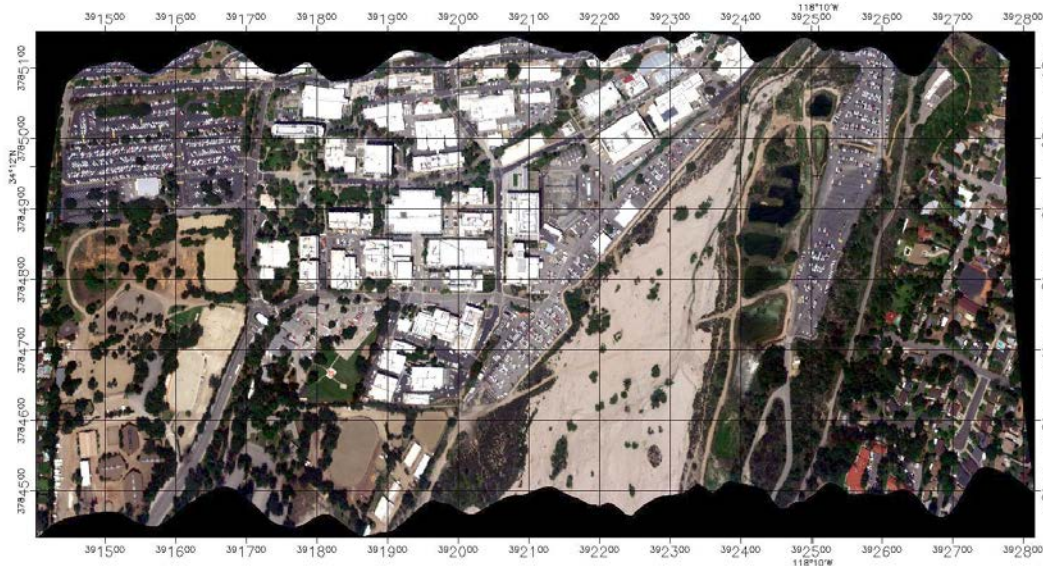


Figure 13. Orthorectified 3-band color image of JPL and surrounding area.

The first calibration site was Ivanpah Playa dry lake in Nevada. Figure 14 shows the lakebed and a blue tarp calibration target. A ground team supported the operation with portable spectrometers and solar photometers. With the combination of ground and solar data it is possible to determine the accuracy with which PRISM recovers spectra, assuming a model of atmospheric absorption. Figure 14 also shows the recorded spectrum of the tarp and the recovered spectrum after atmospheric correction. The spectrum is remarkably smooth at a single integration and without any applied spectral smoothing. The features seen around 900 nm are attributed to uncertainties in the exact atmospheric absorption band location. Ongoing research will resolve this point.

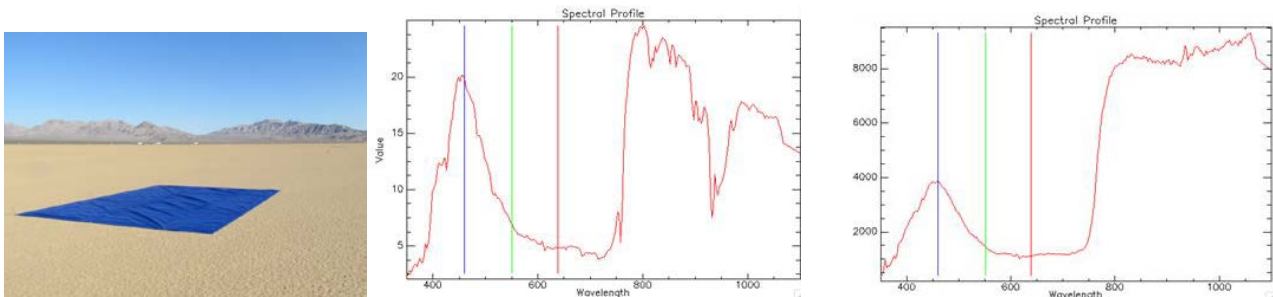


Figure 14. Left: Calibration target (blue tarp) at Ivanpah Playa. Middle: tarp spectrum as seen by PRISM. Right: recovered spectrum after applying radiometric calibration coefficients and atmospheric correction.

A detailed comparison between measured and modeled spectra based on the Ivanpah calibration is shown in Fig. 15, which shows the spectrum of the lakebed as measured by the hand-held spectrometers and as modeled by PRISM using a MODTRAN atmospheric model. There is excellent agreement.

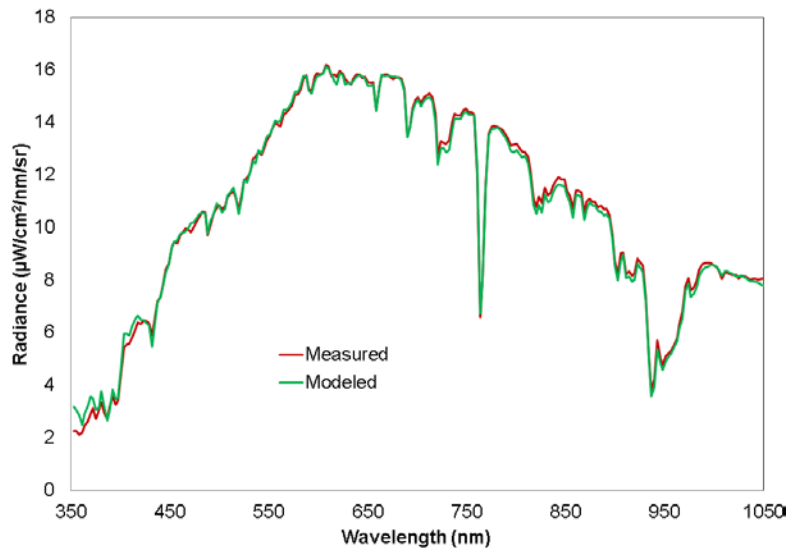


Figure 15. Comparison between measured and modeled lakebed spectra.

The PRISM focal plane readout rate is approximately 168 fps. This fast readout avoids saturation over bright targets given the high optical speed (F/1.8). Depending on the aircraft speed and altitude, this rate means that PRISM will collect several samples over a single IFOV. Those are then summed, which helps increase the SNR. A rather dramatic illustration of this forward oversampling is shown in Fig. 16, where a raw pre-rectified image is compared to the rectified image over the same location at Lake Tahoe. The data from Lake Tahoe overflights are currently under analysis but it is evident that the bottom of the lake is imaged very well by PRISM.

5. CONCLUSIONS

PRISM has demonstrated unique properties and outstanding performance in terms of signal to noise ratio, response uniformity, accurate radiometry, and recovery of high quality spectra. At the time of writing, PRISM had just completed a second flight collecting data over the Monterey Bay area in California. With this additional flight we expect that the instrument will prove its characteristics and demonstrate outstanding data quality in the service of the ocean science community.

ACKNOWLEDGMENTS

This work has been performed at the Jet Propulsion Laboratory, California Institute of Technology, under a contract with the National Aeronautics and Space Administration. Funding has been provided by NASA's Earth Science and Technology Office, and the Airborne Science and Ocean Biology and Biogeochemistry programs. Many individuals contributed to the success of PRISM. We would especially like to acknowledge Dan Wilson, Dave Cohen, Doug Moore, Dave Randall, Ian McCubbin, Frank Loya, Chuck Sarture, Alan Mazer, and Scott Nolte.

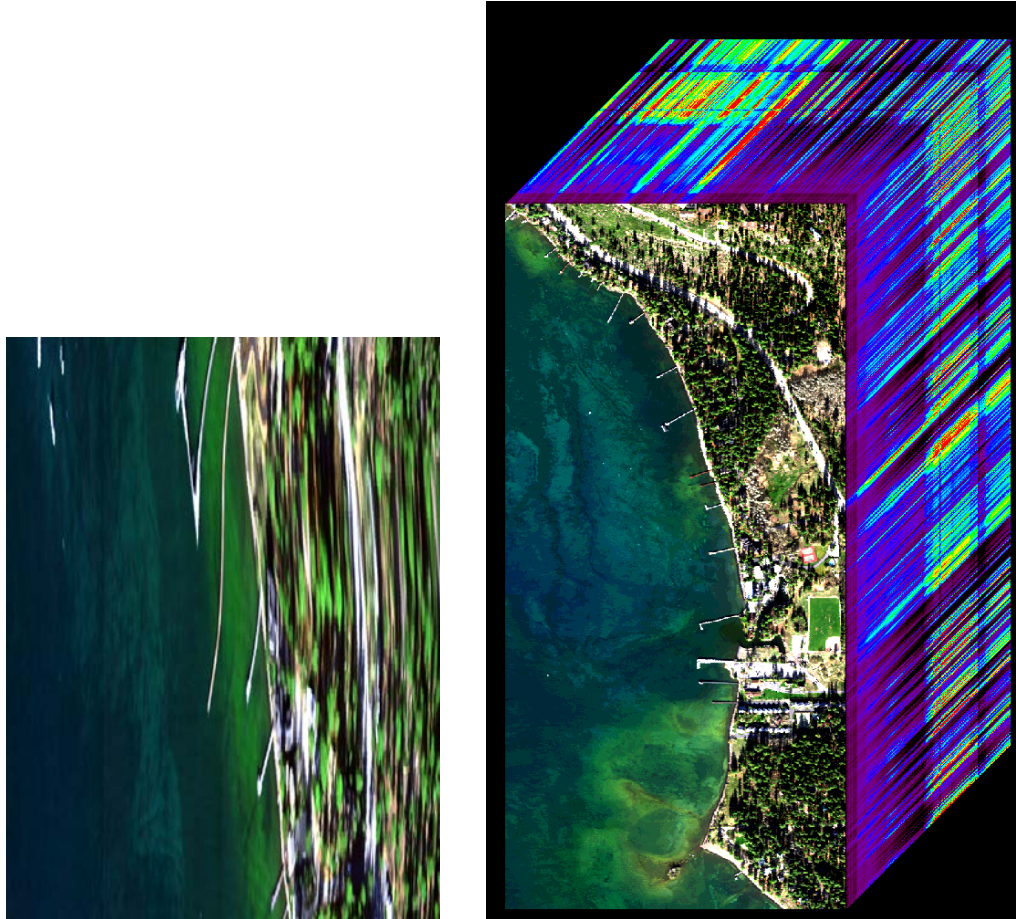


Figure 16. Left: Raw PRISM image showing forward oversampling. Right: orthorectified image cube of a wider area around the Dollar Point coast of Lake Tahoe. Edge pixel spectra are indicated along the depth.

REFERENCES

- [1] Mouroulis, P., Green, R.O., and Wilson, D.W., "Optical design of a coastal ocean imaging spectrometer", *Opt. Express* 16, 9087-9095 (2008).
- [2] Van Gorp, B., Mouroulis, P., Wilson, D., and Balasubramanian, K., "Polarization and stray light considerations for the Portable Remote Imaging Spectrometer (PRISM)", *Proc. SPIE* 7812, 78120R (2010).
- [3] Skauli, T., "An upper-bound metric for characterizing spectral and spatial coregistration errors in spectral imaging," *Opt. Express* 20(2), 918-933 (2012).
- [4] Green, R. O. et al, "Imaging Spectroscopy and the Airborne Visible/Infrared Imaging Spectrometer (AVIRIS)" *Rem. Sens. Environment* 65(3), 227-248 (1998).